

Stability and luminescence properties of $CsPbBr_3$/CdSe/Al core-shell quantum dots

Heng Yao(姚恒), Anjiang Lu(陆安江), Zhongchen Bai(白忠臣),Jinguo Jiang(蒋劲国), and Shuijie Qin(秦水介)
Citation: Chin. Phys. B, 2022, 31 (**4**): 046106. DOI: 10.1088/1674-1056/ac5978
Journal homepage: http://cpb.iphy.ac.cn; http://iopscience.iop.org/cpb

What follows is a list of articles you may be interested in

First-principles study of stability of point defects and their effects on electronic properties of GaAs/AlGaAs superlattice

Shan Feng(冯山), Ming Jiang(姜明), Qi-Hang Qiu(邱启航), Xiang-Hua Peng(彭祥花), Hai-Yan Xiao(肖海燕), Zi-Jiang Liu(刘子江), Xiao-Tao Zu(祖小涛), and Liang Qiao(乔梁)
Chin. Phys. B, 2022, 31 (**3**): 036104. DOI: 10.1088/1674-1056/ac16cb

Effect of structural vacancies on lattice vibration, mechanical, electronic, and thermodynamic properties of Cr_5BSi_3

Tian-Hui Dong(董天慧), Xu-Dong Zhang(张旭东), Lin-Mei Yang(杨林梅), and Feng Wang(王峰)
Chin. Phys. B, 2022, 31 (**2**): 026101. DOI: 10.1088/1674-1056/ac11e2

Probing structural and electronic properties of divalent metal Mg_{n+1} and $SrMg_n$ (n = 2–12) clusters and their anions

Song-Guo Xi(奚松国), Qing-Yang Li(李青阳), Yan-Fei Hu(胡燕飞), Yu-Quan Yuan(袁玉全), Ya-Ru Zhao(赵亚儒), Jun-Jie Yuan(袁俊杰), Meng-Chun Li(李孟春), and Yu-Jie Yang(杨雨杰)
Chin. Phys. B, 2022, 31 (**1**): 016106. DOI: 10.1088/1674-1056/ac04aa

Pressure dependence of the thermal stability in $LiMn_2O_4$

Yan Zeng(曾彦), Hao Liang(梁浩), Shixue Guan(管诗雪), Junpu Wang(王俊普), Wenjia Liang(梁文嘉), Mengyang Huang(黄梦阳), and Fang Peng(彭放)
Chin. Phys. B, 2022, 31 (**1**): 016104. DOI: 10.1088/1674-1056/ac1932

Mechanism of microweld formation and breakage during Cu-Cu wire bonding investigated by molecular dynamics simulation

Beikang Gu(顾倍康), Shengnan Shen(申胜男), and Hui Li(李辉)
Chin. Phys. B, 2022, 31 (**1**): 016101. DOI: 10.1088/1674-1056/ac0e24

Stability and luminescence properties of $CsPbBr_3$/CdSe/Al core-shell quantum dots

Heng Yao(姚恒)[1], Anjiang Lu(陆安江)[1,†], Zhongchen Bai(白忠臣)[1,2], Jinguo Jiang(蒋劲国)[1], and Shuijie Qin(秦水介)[1,‡]

[1] *Guizhou Province Key Laboratory for Photoelectric Technology and Application, Guizhou University, Guiyang* 550025, *China*
[2] *College of Medicine, Guizhou University, Guiyang* 550025, *China*

(Received 27 November 2021; revised manuscript received 26 January 2022; accepted manuscript online 2 March 2022)

To improve the stability and luminescence properties of $CsPbBr_3$ QDs, we proposed a new core-shell structure for $CsPbBr_3$/CdSe/Al quantum dots (QDs). By using a simple method of ion layer adsorption and a reaction method, CdSe and Al were respectively packaged on the surface of $CsPbBr_3$ QDs to form the core-shell $CsPbBr_3$/CdSe/Al QDs. After one week in a natural environment, the photoluminescence quantum yields of $CsPbBr_3$/CdSe/Al QDs were greater than 80%, and the PL intensity remained at 71% of the original intensity. Furthermore, the $CsPbBr_3$/CdSe/Al QDs were used as green emitters for white light-emitting diodes (LEDs), with the LEDs spectrum covering 129% of the national television system committee (NTSC) standard color gamut. The core-shell structure of QDs can effectively improve the stability of $CsPbBr_3$ QDs, which has promising prospects in optoelectronic devices.

Keywords: luminescence properties, stability, $CsPbBr_3$/CdSe/Al quantum dots (QDs), $CsPbBr_3$ QDs

PACS: 61.46.–w, 61.46.Df, 73.63.–b, 78.55.–m **DOI:** 10.1088/1674-1056/ac5978

1. Introduction

Due to their high photoluminescence quantum yields (PLQYs), adjustable emission wavelength, and narrow spectral width, perovskite quantum dots (PQDs) have become a research hotspot in the field of luminescence and have demonstrated tremendous potential in light-emitting diodes (LEDs),[1,2] photodetectors,[3,4] lasers,[5–7] and solar cells.[8,9] By doping halogen anions and controlling the proportion of anions, the all-inorganic lead halide PQDs ($CsPbX_3$, X = Cl, Br, I) can obtain a good emission spectrum and span the entire visible light range.[10,11] Green-emitting $CsPbBr_3$ QDs often exhibit higher PLQYs than blue-emitting $CsPbCl_3$ QDs and red-emitting $CsPbI_3$ QDs, which is helpful for optical device applications.[12]

In general, $CsPbBr_3$ QDs have poor long-term stability, limiting their applications in photovoltaic and optoelectronic devices. The instability of PQDs is mainly attributed to irreversible changes in their surface ligands or chemical structure in the presence of water and oxygen.[13] A variety of solutions have been devised by researchers to improve the stability of PQDs. The surface coating method is considered as one of the most prevalent and effective methods for improving their stability.[14] For example, after coating $CsPbBr_3$ QDs with SiO_2,[15] AlO_X,[16] and TiO_2,[17] the stability of PQDs has been significantly improved. However, these coating materials cause several defects in $CsPbBr_3$ QDs, substantially reducing the PLQYs of $CsPbBr_3$ QDs, affecting their fluorescence intensity and limiting their applicability in optoelectronic devices.[18] As a result, there is an urgent need to develop a novel method for improving the stability of all-inorganic PQDs while maintaining good luminous performance.

CdSe is an excellent photoelectric nanomaterial with a lot of electron interaction with $CsPbBr_3$.[19] When $CsPbBr_3$ QDs and CdSe nanowires are in contact, a spontaneous charge transfer occurs, resulting in a solid binding field of similar p-n junctions.[20] Ghosh *et al.*[21] studied the electron transfer effect between the CdSe nanoplatelet and the $CsPbX_3$ QDs. Their high photocurrent and dark current were both up to 0.04 μA and 62.4 μA, respectively. However, in practical applications, the stability of CdSe and $CsPbBr_3$ QDs binding has not been extensively studied. Few people have worked on improving the stability of $CsPbBr_3$/CdSe QDs. Obtaining stable core/shell structured colloidal PQDs by coating $CsPbBr_3$ QDs with II–VI semiconductors,[22] such as $CsPbBr_3$/CdS[23] and $CsPbBr_3$/ZnS,[24] has been the subject of some research. Moreover, stable QDs were obtained by doping aluminum isopropoxide into CdSe/CdS QDs by using the successive ion layer adsorption and reaction (SILAR) method.[25] As a self-passivation layer on the surface of core-shell QDs, Al can be oxidized to Al_2O_3, effectively preventing photodegradation under long-term light irradiation.[26] As a result of coating $CsPbBr_3$/CdSe QDs with aluminum isopropoxide, it is projected that the PQDs' stability and fluorescence emission intensity will improve.

In this study, CdSe and Al serve as protective shells for

†Corresponding author. E-mail: ajlu@gzu.edu.cn
‡Corresponding author. E-mail: shuijieqin@163.com

© 2022 Chinese Physical Society and IOP Publishing Ltd

$CsPbBr_3$ QDs, allowing for the epitaxial growth of core-shell $CsPbBr_3$/CdSe and $CsPbBr_3$/CdSe/Al QDs. In the natural environment, the stability of $CsPbBr_3$, $CsPbBr_3$/CdSe, and $CsPbBr_3$/CdSe/Al QDs was studied. Furthermore, by combining $CsPbBr_3$/CdSe/Al QDs as a green light source with K_2SiF_6:Mn^{4+} (KSF) and a blue light diode chip, white LED (WLED) devices were fabricated, which exhibited good practical application potential.

2. Materials and methods

2.1. Materials

Aladdin supplied cesium carbonate (Cs_2CO_3, 99.99%), lead bromide ($PbBr_2$, 99.99%), cadmium oxide (CdO, 99.99%), selenium (Se, 99.99%), aluminum isopropoxide ($C_9H_{21}AlO_3$, 98.0%), 1-octadecene (ODE, 90.0%), oleylamine (OLA, 80.0%–90.0%), oleic acid (OA, 90.0%) and n-hexane (C_6H_{14}, AR). They did not need to be purified any more.

2.2. Preparation method

2.2.1. Synthesis of $CsPbBr_3$ QDs

To make a cesium oleate solution, Cs_2CO_3 (0.4 g), ODE (15 mL), and OA (1.25 mL) were placed into a three-neck flask (100 mL) and heated at 150 °C for 1 hour until all the Cs_2CO_3 was completely dissolved. $PbBr_2$ (0.15 g), ODE (10 mL), OA (1 mL) and OLA (1 mL) were all combined in a three-neck flask and heated at 120 °C for 1 hour. The temperature was raised to 150 °C after the $PbBr_2$ power was dissolved. The Cs-oleate solution (2 mL) was then immediately injected. In an ice-water bath, the reaction mixture was cooled to room temperature after 10 s. After centrifugation at 7000 rpm for 10 min to extract the $CsPbBr_3$ QDs, the supernatant was discarded, and the precipitate was dispersed in n-hexane. The supernatant was then centrifuged at 9000 rpm for 10 min to achieve the appropriate PQDs, and the process was repeated twice to obtain the desired PQDs.

2.2.2. Synthesis of $CsPbBr_3$/CdSe QDs

CdO (0.03 g), OA (1.5 mL), and ODE (25 mL) were placed in a three-neck flask and heated at 200 °C for 45 min to produce a Cd $(OAc)_2$ solution. Se (0.14 g), OA (5 mL), and ODE (20 mL) were poured into another three-neck flask and heated at 230 °C for 1 hour to make a Se solution. After the CdSe coating, the Cd $(OAc)_2$ (0.75 mL) and Se (0.75 mL) solutions were injected into the cooled and uncentrifuged $CsPbBr_3$ solution and the reaction was completed by stirring for 5 min. As previously stated, the reaction mixture was centrifuged and washed to yield $CsPbBr_3$/CdSe QDs.

2.2.3. Synthesis of $CsPbBr_3$/CdSe/Al QDs

After heating a three-necked flask containing $C_9H_{21}AlO_3$ (0.4 g), OA (5 mL), and ODE (14 mL) at 230 °C for 1 hour, a transparent Al $(OAc)_3$ was obtained. Following that, 0.75 mL of Al $(OAc)_3$ precursor solution was injected into the synthesized $CsPbBr_3$/CdSe QDs solution to react for 10 min. As previously stated, the reaction mixture was centrifuged and washed to obtain $CsPbBr_3$/CdSe/Al QDs (Fig. 1). Displayed in the support information, pure CdSe QDs were also prepared as a comparison.

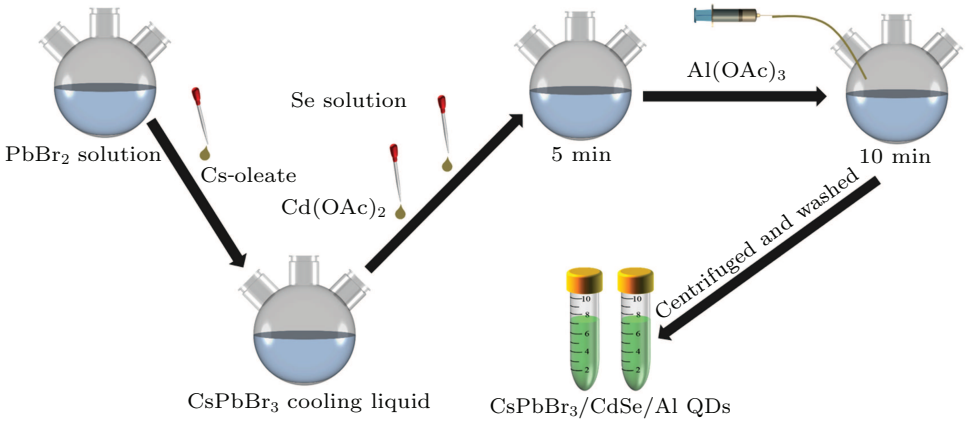


Fig. 1. Schematic diagram of the synthesis of $CsPbBr_3$/CdSe/Al QDs.

2.3. Characterization methods

Transmission electron microscopy (TEM) was used to analyze the morphologies of the diluted $CsPbBr_3$, $CsPbBr_3$/CdSe, and $CsPbBr_3$/CdSe/Al QDs that were dropped on the ultra-thin carbon film copper mesh (JEOL2100F). An optical fiber spectrophotometer was used to record the PL spectra of the samples (Ocean Optics, QE6500). The x-ray diffractometer (XRD) specimens were prepared by drying the diluted QDs in n-hexane on the glass sheet, and the phase structure of QDs was characterized by XRD (Rigaku Smart Lab XG). The components in the sample were obtained by energy-dispersive x-ray (EDX) (X-MAX 80). A Shimadzu UV-2700 UV–Vis spectrophotometer was used to measure the UV–Vis absorption spectra. The samples of the produced

QDs were washed and dried into powder, and x-ray photoelectron spectroscopy (XPS) of the sample was obtained by using Thermo Scientific's ESCALAB 250Xi spectrometer. The surface chemical compositions were measured by a Fourier transform infrared (FTIR) spectrometer (Bruker, V70) equipped with an infrared microscope (H1000). All samples' PLQYs were obtained by dispersing Rhodamine 6G (QYs $\approx$ 95%) in an ethanol solution as a reference dye. A WITec alpha 300R confocal Raman microscopy was used to examine the Raman spectra of QDs. Ultraviolet photoelectron spectroscopy (UPS) of samples were tested by using ESCALAB 210 (VG, UK).

2.4. Fabrication of WLED devices

The PQDs were washed and then vacuum-dried for 24 hours at 60 °C. To obtain homogenous latex, the PQDs powder was mixed with K_2SiF_6:Mn^{4+} (KSF) red phosphors before adding silicone resins A and B (A:B = 1:4) to the beaker. The resulting latex was dropped on the blue light chip and dried in a vacuum drying box at 100 °C for 1 hour to produce the WLED device. The electroluminescent (EL) spectra and chromaticity coordinates of WLED were measured by Rainbow HP9000 at 20 mA forward current.

3. Results and discussion

Figures 2(a)–2(c) showed the TEM morphological images of $CsPbBr_3$, $CsPbBr_3$/CdSe, and $CsPbBr_3$/CdSe/Al QDs. They were all relatively uniform cubic crystal phases, demonstrating that Al had little effect on the QDs' morphology. The sample's morphology was analyzed by using particle size statistics, as illustrated in the upper right corner of Figs. 2(a)–2(c). The average size of $CsPbBr_3$ QDs before coating with CdSe and Al was approximately 8.23 nm, which was close to the radius of its Bohr exciton radius (7 nm). The average size of $CsPbBr_3$/CdSe and $CsPbBr_3$/CdSe/Al QDs was approximately 9.68 nm and 9.95 nm, respectively. Furthermore, Fig. 2(d) showed the high-resolution TEM (HRTEM) image of $CsPbBr_3$/CdSe/Al QDs with obvious lattice fringes, indicating that the prepared samples were highly crystallinity. We measured the lattice spacing to be 0.29 nm and 0.35 nm (inset in Fig. 2(d)), which correspond to the crystal planes of $CsPbBr_3$ (200) and (111) crystal planes of CdSe, respectively. Moreover, only a few CdSe lattice patterns were (marked parts in Fig. 2(d)), which was ascribed to an insufficient sample layer and excessive background noise.

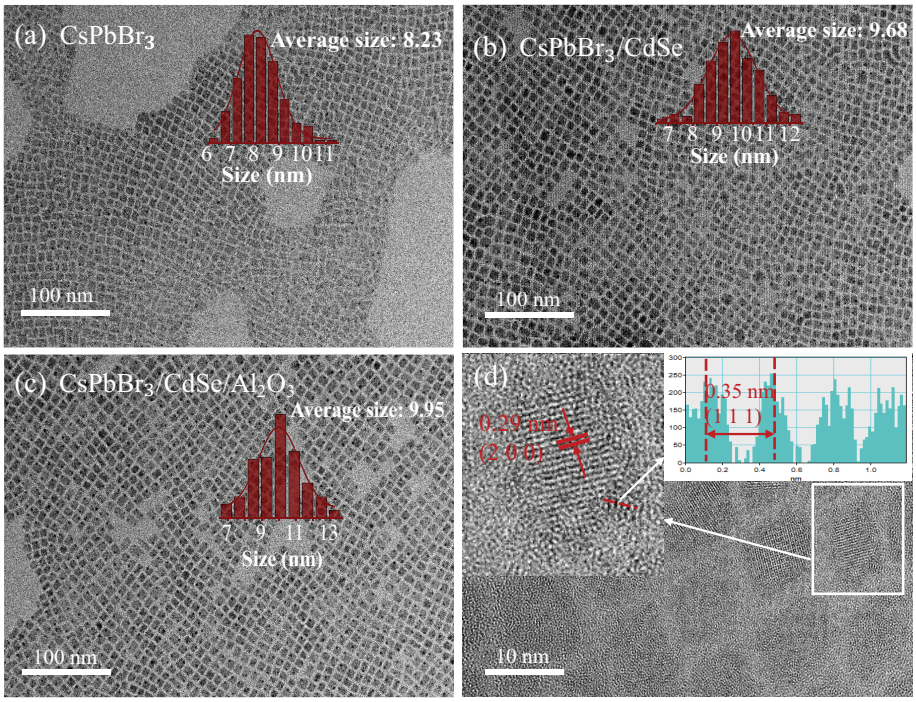


Fig. 2. TEM images of (a) $CsPbBr_3$, (b) $CsPbBr_3$/CdSe and (c) $CsPbBr_3$/CdSe/Al QDs; (d) HRTEM image of the $CsPbBr_3$/CdSe/Al QDs.

To confirm the structure of $CsPbBr_3$/CdSe/Al QDs further, the phase structure of QDs was determined using XRD, as illustrated in Fig. 3(a). In comparison to the conventional PDF card data for $CsPbBr_3$ (PDF#18-0364) and CdSe (PDF#19-0191), we observed diffraction peaks for $CsPbBr_3$ (001), (110), and (200), as well as CdSe (111), indicating that the $CsPbBr_3$/CdSe structure was successfully synthesized. However, no Al diffraction peaks were seen in the XRD spectra, and we speculated that the aluminum coating had not undergone an oxidation process and the concentration was low. Simultaneously, the introduction of the shell changed the entire XRD diffraction spectra, which had shifted slightly towards large angles. This slight shift was attributed to the larger Pb^{2+} ion's (119 μm) displacement by the smaller Cd^{2+} ion (97 μm).

Meanwhile, single-element line scans of $CsPbBr_3$/CdSe/Al QDs were tested (Fig. 2(b)), and the results showed that the Se, Cd, and Al elements had relatively high counts at the ends of their shell layers, which further demonstrated the formation of the core-shell structure. The corresponding EDX spectral analysis (Fig. 2(c)) confirmed the presence of Cs, Pb, Br, Se, Cd, and Al elements, and confirmed that the appearance of Cu was due to the copper mesh substrate. By comparing the HRTEM images of $CsPbBr_3$ and $CsPbBr_3$/CdSe/Al, Fig. S3 demonstrate that the cubes' corner points become circular, implying the formation of the core-shell structure. The thickness of the shell layer was about 1.2 nm (the enlargement of Fig. S3), indicating that the size increase was caused by the coating of CdSe and Al.

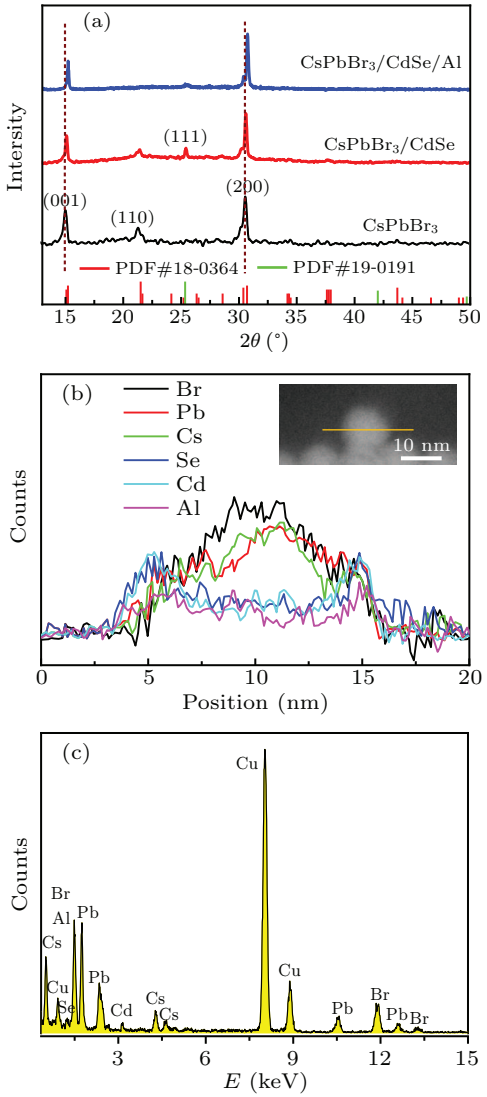


Fig. 3. (a) XRD spectra of $CsPbBr_3$, $CsPbBr_3$/CdSe and $CsPbBr_3$/CdSe/Al QDs; (b) EDX line profiles of Br, Pb, Cs, Cd, Se, and Al for the $CsPbBr_3$/CdSe/Al QDs; (c) EDX spectra of the $CsPbBr_3$/CdSe/Al QDs.

All the samples were excited at 365 nm by the pump light to acquire their PL spectra, as shown in Fig. 4(a). When compared to $CsPbBr_3$, the PL peaks of $CsPbBr_3$/CdSe and $CsPbBr_3$/CdSe/Al QDs exhibited a slight redshift ($\sim$ 5 nm) and a slight enhancement in PL intensity. CdSe's PL spectrum was not observed, most likely because the CdSe layer was too thin and absorbed much less light than the $CsPbBr_3$ QDs. When the PL spectrogram was enlarged, the QDs coated with CdSe showed shoulder peaks of about 560 nm (Fig. S4(a)). Additionally, when compared to naked $CsPbBr_3$, the sample's full width at half-maximum was narrower following CdSe and Al coating, indicating a more uniform size and crystallinity. Figure 4(a) also showed the absorption spectra of QDs, whose absorption edge corresponded well to the PL emission peak. There was a slight Stokes shift between the absorption peak and the PL emission peak, indicating that the luminescence of QDs is primarily due to the radiative recombination of free or bound excitons.[27] The PLQYs of $CsPbBr_3$, $CsPbBr_3$/CdSe, and $CsPbBr_3$/CdSe/Al QDs were documented in Table 1. Around 79.0%, 80.4%, and 80.2%, respectively. The absorption of light by QDs and the radiation complex of excitons define the value of PLQYs. While the addition of CdSe could passivate the defects of $CsPbBr_3$ to enhance the radiation complex, the absorption of light by QDs was almost not increased (Fig. S5). Since a part of the excitation light was absorbed by CdSe, the absorption of light by $CsPbBr_3$ QDs was weakened, resulting in a minimal difference in PLQYs. This indicates that the core-shell QDs created have exceptional luminous properties as well.

Table 1. PLQYs of $CsPbBr_3$, $CsPbBr_3$/CdSe, and $CsPbBr_3$/CdSe/Al QDs.

Samples	PLQYs (%)
$CsPbBr_3$ QDs	79.0%
$CsPbBr_3$/CdSe QDs	80.4%
$CsPbBr_3$/CdSe/Al QDs	80.2%

The comparative Raman spectra of the $CsPbBr_3$ and $CsPbBr_3$/CdSe were showed in Fig. 4(b). Three Raman vibrational peaks for $CsPbBr_3$ were detected, with a sharp peak at 75.5 cm^{-1} and wide peaks at 127 cm^{-1} and 306 cm^{-1}. The peaks at 75.5 cm^{-1} and 124 cm^{-1} were classified as $[PbBr_6]^{4-}$ octahedral vibration mode and Cs^+ cation movement.[28,29] The weak broadband at 306 cm^{-1} was related to the second-order phonon mode of the octahedron.[28,29] Notably, the $CsPbBr_3$/CdSe QDs exhibited an additional micro peak near 206 cm^{-1}, which corresponds to the first-order CdSe longitudinal optical phonon mode,[30] and the sharp peak of the $CsPbBr_3$/CdSe QDs located at 75.5 cm^{-1} exhibited a distinct redshift ($\sim$ 3 cm^{-1}). The redshift in the characteristic peak position indicated the $CsPbBr_3$ and CdSe interacted and transferred charge.[31,32] Figure 4(c) shows the UPS spectra of $CsPbBr_3$ and CdSe QDs. The secondary electron cutoff edge of $CsPbBr_3$ and CdSe QDs was determined to be 16.87 eV and 17.82 eV, respectively (the left half of Fig. 4(c)). From this, the Fermi energy level (E_F) and work function (Φ) can be calculated from the secondary energy cutoff edge: $\Phi = 21.22$ eV –

secondary electron cutoff edge (21.22 eV is the excitation energy of the helium source). Thus, the Φ of $CsPbBr_3$ and CdSe are 4.35 eV and 3.4 eV, respectively, while the Fermi energy levels of $CsPbBr_3$ and CdSe are −4.35 eV and −3.4 eV, respectively. The abscissa of the front edge of the valence band was intersected with the extension of the background channel and was used to determine the valence band maximum (E_V). The deduced E_{Vs} were 1.57 eV and 1.43 eV for $CsPbBr_3$ and CdSe QDs, respectively (the right half of Fig. 4(c)). The bandgap was obtained by analyzing the UV–vis absorption spectra (Fig. S4(b)) of $CsPbBr_3$ and CdSe QDs.

In light of the aforementioned results, an equilibrium energy band diagram for the $CsPbBr_3$/CdSe interface was proposed (Fig. 4(d)). Figure S6 showed the energy band diagram of the $CsPbBr_3$/CdSe QDs prior to contact. This result was similar to previous studies.[20,21] At the contact between the $CsPbBr_3$ core and the CdSe shell, a core-shell heterojunction was theoretically and apparently created at the interface. As a result, Fig. 4(d) might be used to describe the possible physical mechanism by which $CsPbBr_3$/CdSe/Al QDs enhance their fluorescence. Following that, $CsPbBr_3$ QDs were coated with CdSe to form $CsPbBr_3$/CdSe QDs with a core-shell structure. $CsPbBr_3$/CdSe QDs induce photogenerated carriers upon the excitation of 365 nm pump light. Because $CsPbBr_3$ has a lower E_F than CdSe, electrons flow from CdSe's conduction band to $CsPbBr_3$. At the interface of $CsPbBr_3$/CdSe, the electron accumulation layer formed on one side of $CsPbBr_3$ and the depletion layer formed on the other side of CdSe. Due to the inflow of electrons from the CdSe shell, the surface defects of $CsPbBr_3$ QDs were passivated, promoting carrier radiative recombination. As a result, the fluorescence intensity of $CsPbBr_3$ QDs was enhanced after coating. Meanwhile, the redshift of the PL spectra might be due to the spreading of the electron wave function of the $CsPbBr_3$ quantum dot to the CdSe shell layer.[24,33] The possibility of a radiative transition from the CdSe conduction band to the $CsPbBr_3$ valence band caused the absorption and emission wavelength of these structures to be strongly shifted towards lower energies. This bandgap reduction lowers the energy of excitons (also confinement energy), leading to redshift in the PL and absorption spectra of the $CsPbBr_3$/CdSe core-shell structure.[34] The $CsPbBr_3$/ZnS,[24] $CsPbBr_3$/CdS,[35] and CdSe/ZnS[36] core-shell structures all exhibit similar redshift in the PL spectra.

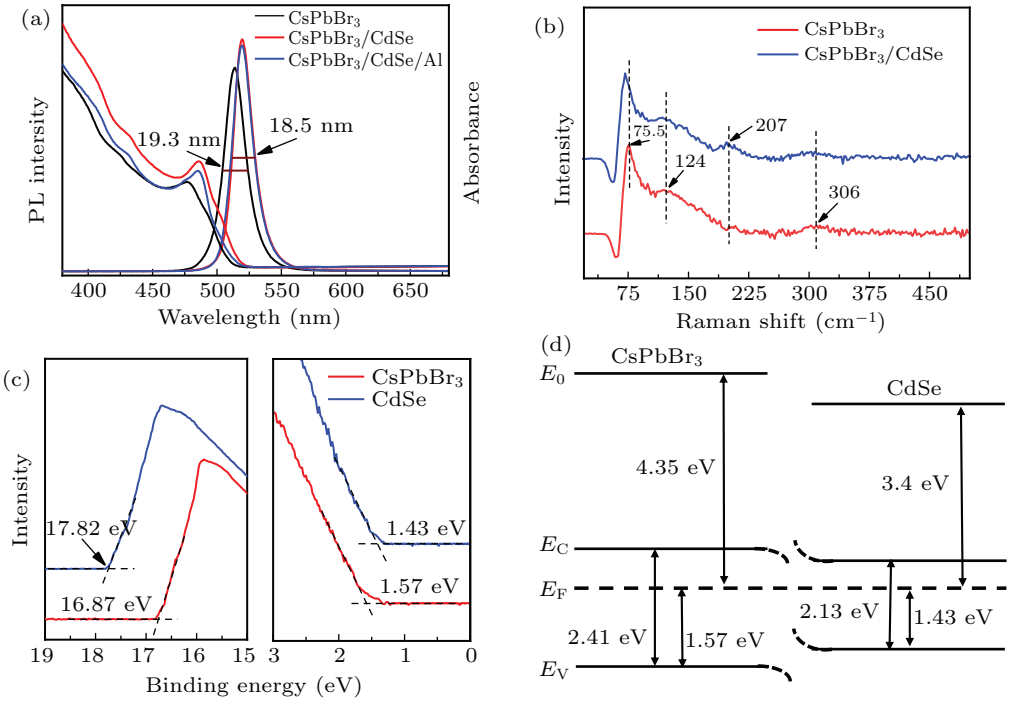


Fig. 4. (a) PL spectra and UV–vis spectra of $CsPbBr_3$, $CsPbBr_3$/CdSe and $CsPbBr_3$/CdSe/ Al QDs; (b) Raman spectra of $CsPbBr_3$, $CsPbBr_3$/CdSe; (c) UPS spectra of $CsPbBr_3$ and CdSe QDs; (d) energy-level diagram of $CsPbBr_3$/CdSe QDs.

The stability of $CsPbBr_3$, $CsPbBr_3$/CdSe, and $CsPbBr_3$/CdSe/Al QDs was determined by the PL intensity of the samples in the next week in the natural environment, as shown in Figs. 5(a)–5(c). We observed that $CsPbBr_3$ QDs were extremely sensitive to light and water in the air, with the PL intensity gradually decreasing to 23% of the original intensity after a week in the natural environment (Fig. 5(d)). Additionally, the $CsPbBr_3$/CdSe QDs also rapidly declined to 42% of their original intensity. On the contrary, the PL intensity of $CsPbBr_3$/CdSe/Al QDs decayed relatively slowly in the natural environment, remaining at 71% of the original intensity after a week. Additionally, as illustrated in Fig. 5(d), the $CsPbBr_3$, $CsPbBr_3$/CdSe, and $CsPbBr_3$/CdSe/Al QDs initially demonstrated an obvious green solution in their natural

environment. Due to the absorbing photons, a large amount of yellow precipitation formed on the surface of $CsPbBr_3$ and $CsPbBr_3$/CdSe QDs. Some binding ligands on the surface were removed and the crystal agglomerated, causing the crystal size to increase. However, only a trace of precipitation appeared on the surface of $CsPbBr_3$/CdSe/Al QDs due to the Al_2O_3 self-passivation layer formed by aluminum on the surface of $CsPbBr_3$/CdSe QDs. Not only did the passivation layer inhibit the oxidation reaction between O_2 and PQDs, it also inhibited the adsorption of water molecules in the air on the surface of PQDs, thus reducing the PQD reunion.[37–39]

To gain a better understanding of how aluminum changes on the surface of $CsPbBr_3$/CdSe/Al QDs, we studied the XPS spectra (Fig. 6(a)). Cs 3d, Pb 4f, Br 3d, Se 3d, Cd 3d, Al 2p, and C 1s were detected in the XPS spectra of the $CsPbBr_3$/CdSe/Al QDs showed some distinct peaks. These results were consistent with those reported in the literature.[40–42] C is primarily a result of hydrocarbon pollutants in XPS.[43] Figure 6(b) shows the high-resolution XPS spectra of Al 2p (74.5 eV), which was connected to the Al in the Al–O and Al–OH bonds.[26,44,45] After five days, the Al 2p peak changed to a smaller binding energy direction, owing to the conversion of Al–OH bonds into Al–O bonds.[26,46] Figure 6(c) shows the high-resolution XPS spectra of O 1s. The O 1s peak was found at 531.3 eV in the $CsPbBr_3$/CdSe/Al QDs spectrum, and deconvoluted the spectrum into two peaks with binding energies of 532.7 eV and 531.2 eV, respectively. The peak near 531.2 eV was traditionally attributed to the O 1s energy level in the Al–O bond of Al_2O_3, whereas the peak at 532.7 eV corresponds to the O 1s energy level in the Al–OH bond of $Al(OH)_3$.[47–49] Interestingly, after five days, the peak at 531.2 eV progressively increased while the peak at 532.7 eV gradually faded, indicating that $Al(OH)_3$ would eventually dehydrate to become Al_2O_3 in the natural environment, and the Al_2O_3 layer had anti-oxidation and photodegradation properties.[26,46] As a result, the stability of the $CsPbBr_3$ QDs was significantly improved following the addition of Al.

Figure 6(d) shows the FTIR spectra of $CsPbBr_3$/CdSe/Al QDs. The vibration peak near 800 cm^{-1} was attributed to the vibration of the Al–O bond in Al_2O_3,[25,50] confirming that aluminum isopropoxide had been oxidized to Al_2O_3 on the surface of QDs. The peaks at 2924 cm^{-1} and 2854 cm^{-1} were attributed to the stretching vibration of the C–H bond, whereas the peaks at 3423 cm^{-1} and 3076 cm^{-1} were caused by the vibration of H–O and $–NH_2$, respectively. The stretching vibration of C=C and C–C bonds yielded peaks of 1641 cm^{-1} and 1255 cm^{-1}, respectively. The peak at 1465 cm^{-1} was caused by the asymmetric angular vibration of $–CH_3$, whereas the peak at 910 cm^{-1} was generated by the C–O–H bond's out-of-plane bending vibration. These bonds indicated that, in addition to Al_2O_3, some OA and OLA were present on the surface of QDs. At 2362 cm^{-1}, the peak was from CO_2 molecules in the test environment.

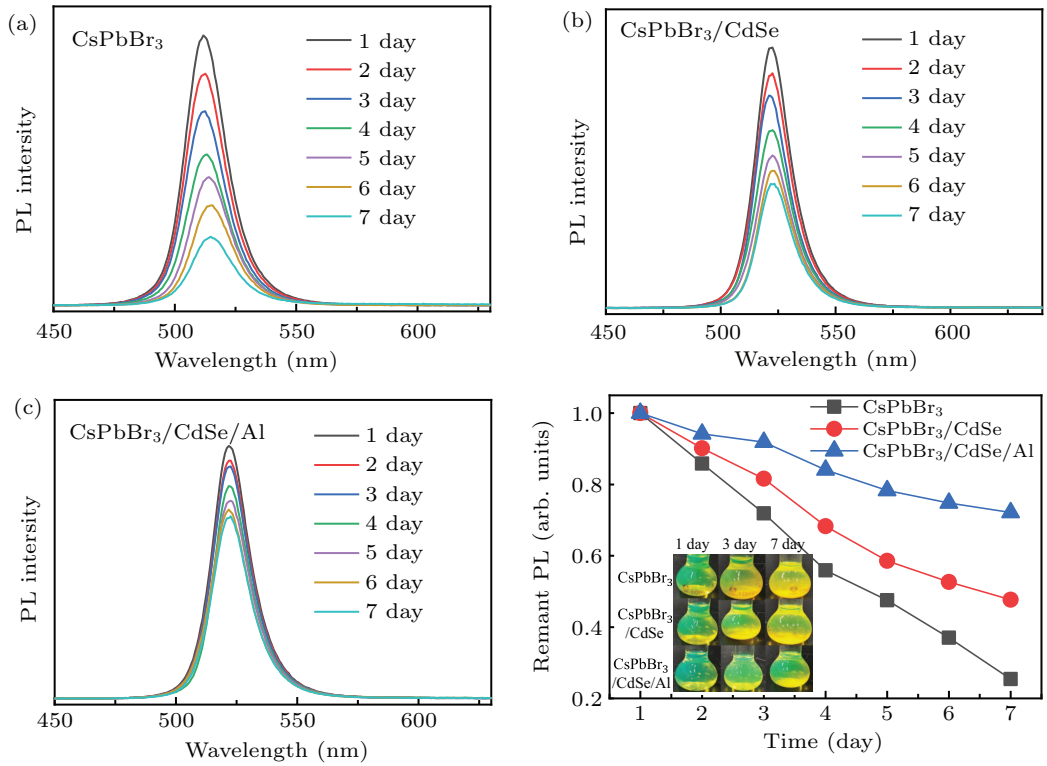


Fig. 5. Stability of (a) $CsPbBr_3$, (b) $CsPbBr_3$/CdSe and (c) $CsPbBr_3$/CdSe/Al QDs in the natural environment by monitoring the relative PL intensity of the samples; (d) the comparison of relative PL intensity for the three samples.

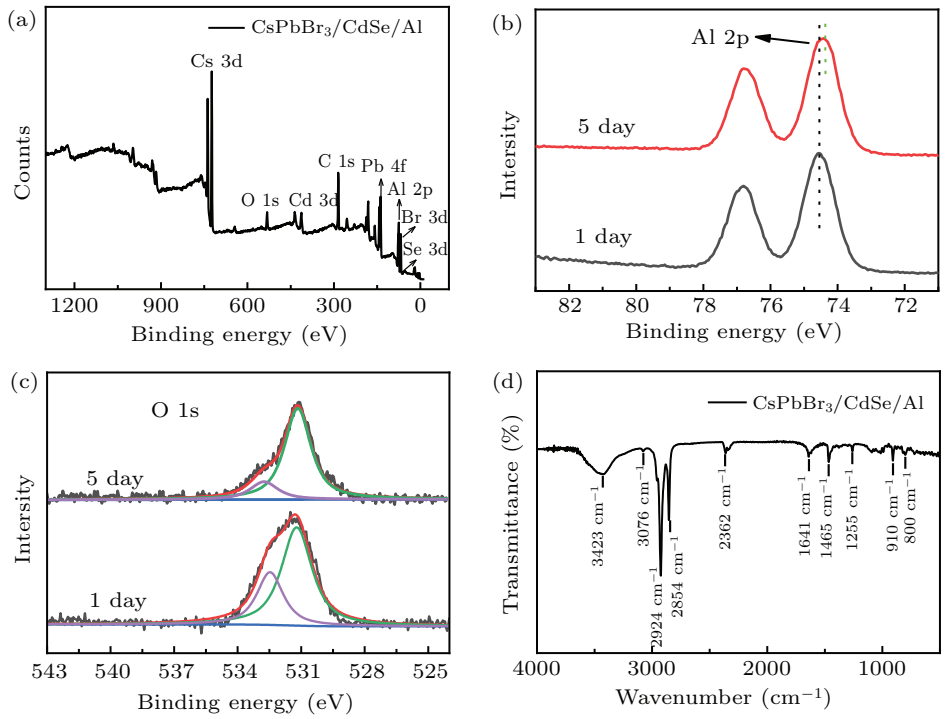


Fig. 6. (a) The XPS spectrum of $CsPbBr_3$/CdSe/Al QDs; (b) Al 2p and (c) O 1s high-resolution XPS spectra of $CsPbBr_3$/CdSe/Al QDs (one day later and five days later); (d) FTIR spectrum of $CsPbBr_3$/CdSe/Al QDs.

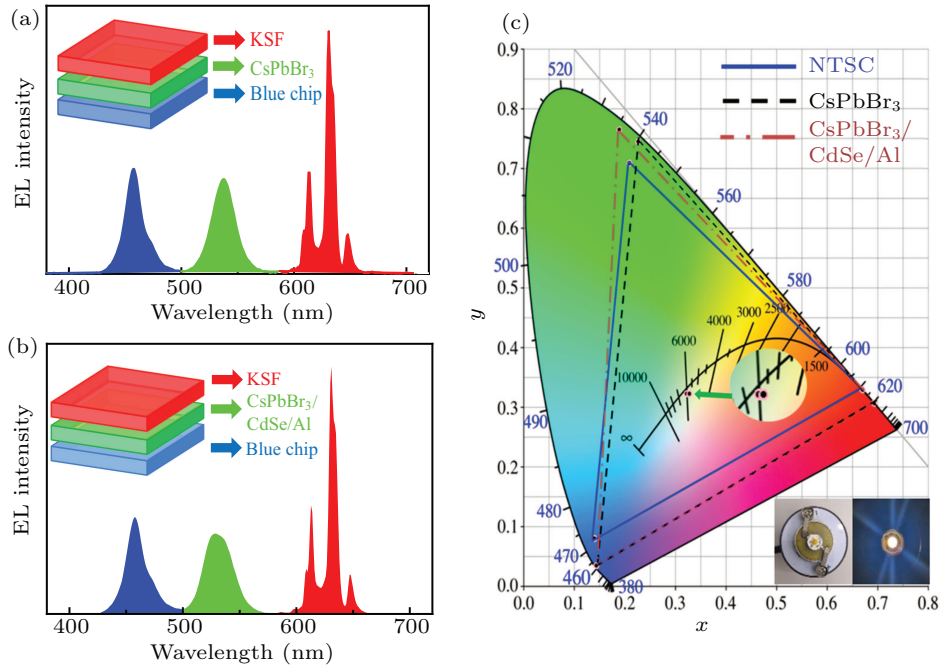


Fig. 7. EL spectra of the constructed WLED based on (a) $CsPbBr_3$ and (b) $CsPbBr_3$/CdSe/Al QDs. (c) The color gamut and color coordinates of the white LED systems in CIE 1931.

The produced $CsPbBr_3$ and $CsPbBr_3$/CdSe/Al QDs were used as green luminescence in WLED devices due to their good luminescence properties. The WLED device was constructed by coating a blue light chip with QDs and a red phosphor KSF (460 nm). Figures 7(a) and 7(b) show the device structure and EL spectra of the WLED device with a current of 20 mA. The characteristics of WLEDs are presented in Table 2. The color rendering index of the WLEDs fabricated with $CsPbBr_3$ and $CsPbBr_3$/CdSe/Al QDs was both 67.1, and the CIE 1931 chromaticity coordinates were (0.328, 0.323) and (0.322, 0.323), respectively (Fig. 7(c)), which were close to the standard white light emission coordinates (0.33, 0.33). And their corresponding color temperatures were 5809 K and 6060 K, respectively, for cold white light. Additionally, the triangular gamut of WLED devices based on $CsPbBr_3$ and $CsPbBr_3$/CdSe/Al QDs could cover 116% and

129% of the National Television System Committee (NTSC) standard color, respectively. Figure 7(c) illustrates two digital photos of the fabricated device in both its operational and non-operational phases. These optical values reflected that $CsPbBr_3$/CdSe/Al QDs retained the excellent luminous properties of $CsPbBr_3$ QDs. It is a great potential application for lighting and backlight down converters for liquid crystal displays.

Table 2. Optical parameters of WLEDs.

Samples	CRI	Chromaticity coordinate	CCT (K)	Cover NTSC
$CsPbBr_3$	67.1	(0.328, 0.323)	5809	116%
$CsPbBr_3$/CdSe/Al	67.1	(0.322, 0.323)	6060	129%

4. Conclusion

In summary, we used the thermal injection approach to synthesize $CsPbBr_3$ QDs and $CsPbBr_3$/CdSe and $CsPbBr_3$/CdSe/Al QDs by the SILAR method. CdSe and Al_2O_3 shells are utilized to encapsulate $CsPbBr_3$ QDs, greatly upgrading their resistance of the $CsPbBr_3$ QDs to water molecules and O_2 in the air and stabilizing their luminescence. After a week in the natural environment, we observed that $CsPbBr_3$/CdSe/Al QDs exhibited high PLQYs (80.2%) and maintained 71% of their original photoluminescence intensity. The WLED device was fabricated by using $CsPbBr_3$/CdSe/Al QDs quantum dots as a green light source that covered 129% of the NTSC color range. This study proposed a novel structure to stabilize $CsPbBr_3$ QDs, which resulted in a significant improvement in luminescence and stability. This research establishes a benchmark for the practical application of $CsPbBr_3$ QDs in optoelectronic devices.

Acknowledgements

This work was supported by the National Natural Science Foundation of China (Grant Nos. 61865002 and 62065002); Project of Outstanding Young Scientific and Technological Talents of Guizhou Province, China (Grant No. QKEPTRC [2019]5650); Guizhou Province Science and Technology Platform and Talent Team Project, China (Grant No. QKEPTRC[2018]5616); and Central Government of China Guiding Local Science and Technology Development Plan (Grant No. QKZYD[2017]4004).

References

[1] Quan L N, Rand B P, Friend R H, Mhaisalkar S G, Lee T W and Sargent E H 2019 *Chem. Rev.* **119** 7444
[2] Wei Y, Xu Y, Wang Q, Wang J, Lu H and Zhu J 2020 *Chem. Commun. (Camb)* **56** 5413
[3] Feng J G, Gong C, Gao H F, Wen W, Gong Y J, Jiang X Y, Zhang B, Wu Y C, Wu Y S, Fu H B, Jiang L and Zhang X 2018 *Nat. Electron.* **1** 404
[4] Chu W, Saidi W A, Zhao J and Prezhdo O V 2020 *Angew Chem. Int. Ed. Engl.* **59** 6435
[5] Veldhuis S A, Boix P P, Yantara N, Li M, Sum T C, Mathews N and Mhaisalkar S G 2016 *Adv. Mater.* **28** 6804
[6] Li Y, Shi Z F, Li X J and Shan C X 2019 *Chin. Phys. B* **28** 017803
[7] Liu Z, Li C, Shang Q Y, Zhao L Y, Zhong Y G, Gao Y, Du W N, Mi Y, Chen J, Zhang S, Liu X F, Fu Y S and Zhang Q 2018 *Chin. Phys. B* **27** 114209
[8] Chen B, Rudd P N, Yang S, Yuan Y and Huang J 2019 *Chem. Soc. Rev.* **48** 3842
[9] Yoo J J, Wieghold S, Sponseller M C, Chua M R, Bertram S N, Hartono N T P, Tresback J S, Hansen E C, Correa-Baena J P, Bulovic V, Buonassisi T, Shin S S and Bawendi M G 2019 *Energ. Environ. Sci.* **12** 2192
[10] Nedelcu G, Protesescu L, Yakunin S, Bodnarchuk M I, Grotevent M J and Kovalenko M V 2015 *Nano Lett.* **15** 5635
[11] Wang P, Bai X, Sun C, Zhang X Y, Zhang T Q and Zhang Y 2016 *Appl. Phys. Lett.* **109** 063106
[12] Ramasamy P, Lim D H, Kim B, Lee S H, Lee M S and Lee J S 2016 *Chem. Commun. (Camb)* **52** 2067
[13] Liu J H, Yang Z X, Ye B Q, Zhao Z W, Ruan Y S, Guo T L, Yu X B, Chen G X and Xu S 2019 *J. Mater. Chem. C* **7** 4934
[14] Wei Y, Cheng Z and Lin J 2019 *Chem. Soc. Rev.* **48** 310
[15] Zhong Q, Cao M, Hu H, Yang D, Chen M, Li P, Wu L and Zhang Q 2018 *ACS Nano* **12** 8579
[16] Loiudice A, Saris S, Oveisi E, Alexander D T L and Buonsanti R 2017 *Angew. Chem. Int. Ed. Engl.* **56** 10696
[17] Li Z J, Hofman E, Li J, Davis A H, Tung C H, Wu L Z and Zheng W 2018 *Adv. Funct. Mater.* **28** 1704288
[18] Li J, Xu L, Wang T, Song J, Chen J, Xue J, Dong Y, Cai B, Shan Q, Han B and Zeng H 2017 *Adv. Mater.* **29** 1603885
[19] Brumberg A, Diroll B T, Nedelcu G, Sykes M E, Liu Y, Harvey S M, Wasielewski M R, Kovalenko M V and Schaller R D 2018 *Nano Lett.* **18** 4771
[20] Dey S, Cohen H, Pinkas I, Lin H, Kazes M and Oron D 2019 *J. Chem. Phys.* **151** 174704
[21] Ghosh G, Dutta A, Ghosh A, Ghosh S and Patra A 2020 *J. Phys. Chem. C* **124** 10252
[22] Ahmed G H, Yin J, Bakr O M and Mohammed O F 2021 *Acs Energy Lett.* **6** 1340
[23] Tang X, Yang J, Li S, Liu Z, Hu Z, Hao J, Du J, Leng Y, Qin H, Lin X, Lin Y, Tian Y, Zhou M and Xiong Q 2019 *Adv. Sci. (Weinh)* **6** 1900412
[24] Ravi V K, Saikia S, Yadav S, Nawale V V and Nag A 2020 *Acs Energy Lett.* **5** 1794
[25] Li Z C, Yao W, Kong L, Zhao Y X and Li L 2015 *J. Am. Chem. Soc.* **137** 12430
[26] Koh S, Lee H, Lee T, Park K, Kim W J and Lee D C 2019 *J. Chem. Phys.* **151** 144704
[27] Liu X, Zhang X, Yu S, Li L, Xu J, Gong X, Ding R, Zhang J and Yin H 2020 *Nanotechnology* **31** 375703
[28] Cha J H, Han J H, Yin W, Park C, Park Y, Ahn T K, Cho J H and Jung D Y 2017 *J. Phys. Chem. Lett.* **8** 565
[29] Calistru D M, Mihut L, Lefrant S and Baltog I 1997 *J. Appl. Phys.* **82** 5391
[30] Tschirner N, Lange H, Schliwa A, Biermann A, Thomsen C, Lambert K, Gomes R and Hens Z 2012 *Chem. Mat.* **24** 311
[31] Muduli S, Pandey P, Devatha G, Babar R, M T, Kothari D C, Kabir M, Pillai P P and Ogale S 2018 *Angew. Chem.* **130** 7808
[32] Wang X, He J, Li J, Lu G, Dong F, Majima T and Zhu M 2020 *Appl. Catalysis B* **277** 119230
[33] Lee J S, Kovalenko M V, Huang J, Chung D S and Talapin D V 2011 *Nat. Nanotech.* **6** 348
[34] Smith A M and Nie S 2010 *Acc. Chem. Res.* **43** 190

[35] Hunsur Ravikumar C, Maroli N, Kulkarni B, Kolandaivel P and Balakrishna R G 2022 *Mater. Sci. Engin.* **275** 115513
[36] Niculescu E C and Cristea M 2013 *J. Lumin.* **135** 120
[37] Huang S, Li Z, Kong L, Zhu N, Shan A and Li L 2016 *J. Am. Chem. Soc.* **138** 5749
[38] Li X, Cao F, Yu D, Chen J, Sun Z, Shen Y, Zhu Y, Wang L, Wei Y, Wu Y and Zeng H 2017 *Small* **13** 1603996
[39] Wang Y, Li X, Sreejith S, Cao F, Wang Z, Stuparu M C, Zeng H and Sun H 2016 *Adv. Mater.* **28** 10637
[40] Sun C, Zhang Y, Ruan C, Yin C, Wang X, Wang Y and Yu W W 2016 *Adv. Mater.* **28** 10088
[41] Ospina R, Rincón-Ortiz S A and Rodriguez-Pereira J 2020 *Surface Sci. Spectra* **27** 014021
[42] Tago T, Kataoka N, Tanaka H, Kinoshita K and Kishida S 2017 *Procedia Engin.* **216** 175
[43] Xiang Q, Meng G F, Zhang Y, Xu J Q, Xu P C, Pan Q Y and Yu W J 2010 *Sensor Actuat B* **143** 635
[44] Loginova E, Cosandey F and Madey T E 2007 *Surface Sci.* **601** L11
[45] Shavorskiy A, Muller K, Newberg J T, Starr D E and Buhm H 2014 *J. Phys. Chem. C* **118** 29340
[46] Li Z, Yao W, Kong L, Zhao Y and Li L 2015 *J. Am. Chem. Soc.* **137** 12430
[47] Gao Y F, Nagai M, Masuda Y, Sato F, Seo W S and Koumoto K 2006 *Langmuir* **22** 3521
[48] Cai N, Zhou G, Muller K and Starr D E 2011 *Phys. Rev. Lett.* **107** 035502
[49] Chenakin S P, Silvy R P and Kruse N 2012 *Topics in Catalysis* **55** 731
[50] Loiudice A, Strach M, Saris S, Chernyshov D and Buonsanti R 2019 *J. Am. Chem. Soc.* **141** 8254